Lithium-ion Migration in Layered $Li_{1.06}Ni_{0.5}Co_{0.2}Mn_{0.3}O_2$ Cathode Materials Synthesized at Different Temperatures

Zi-Zhen Xu[1], Yi-Jie Gu[1,*], Hong-Quan Liu[1], Yun-Bo Chen[1], Meng-Chang Lin[2,*]

[1] College of Materials Science and Engineering, Shandong University of Science and Technology, Qingdao 266510, China
[2] College of Electronic Engineering and Automation, Shandong University of Science and Technology, Qingdao 266510, China
[*]E-mail: 13792900643@163.com, mengchanglin@sdust.edu.cn

We examined the effects of synthesis temperature on the structural and electrochemical properties of layered $Li_{1.06}Ni_{0.5}Co_{0.2}Mn_{0.3}O_2$ cathode materials synthesized by co-precipitation. Scanning electron microscopy showed that a higher synthesis temperature resulted in a bigger primary particle size. Rietveld refinement revealed that the content of nickel ions at the 3b site decreased from 0.041 to 0.038 and subsequently increased to 0.064 as synthesis temperature rose from 800 to 980 °C. The incircle/circumcircle radii of the tetrahedral sites providing space for lithium-ion migration increased gradually with synthesis temperature. The $Li_{1.06}Ni_{0.5}Co_{0.2}Mn_{0.3}O_2$ sample synthesized at 920 °C displayed the optimal electrochemical performance, delivering a discharge capacity of 181.6 $mAhg^{-1}$ and initial coulombic efficiency of 84.2% at 0.1C between 2.5 and 4.5 V. Our analysis indicates that the level of cation mixing and the incircle/circumcircle radii of tetrahedral sites in $LiNi_xCo_yMn_zO_2$ are the main factors that affect its electrochemical performance rather than primary particle size.

1. INTRODUCTION

To relieve environmental deterioration and energy shortage issues, rechargeable batteries have become the most attractive power source because of their high energy density [1-2]. At present, $LiCoO_2$ is widely used as the cathode material in commercial lithium-ion batteries [3-4]. However, the high cost, toxicity of Co, and potential safety risks of $LiCoO_2$ restrict its long-term development [5]. Consequently, considerable effort has been devoted to exploring alternative cathode materials to $LiCoO_2$ to obtain lithium-ion batteries with superior performance [6]. Amongst these candidate cathode compounds, layered $LiNi_xCo_yMn_zO_2$ shows outstanding advantages like high capacity, good

cycling stability, and excellent safety performance, so it has drawn the attention of many researchers [7-9].

The performance of $LiNi_xCo_yMn_zO_2$, including its charge–discharge capacity, cycling performance, initial coulomb efficiency, and rate capability, is strongly influenced by the synthesis temperature during synthesis [10-11]. Using an appropriate synthesis temperature can restrain the cation mixing phenomenon in which Li^+ and Ni^{2+} are exchanged between the transition metal and lithium layers. This mixing phenomenon disrupts the lithium-ion diffusion pathways and results in inferior electrochemical performance [12-14]. In addition, adjusting synthesis temperature can change the particle size of materials. A large particle size is a disadvantage for lithium-ion diffusion because of the lower specific surface area of larger particles compared with that of smaller ones [15-16]. Conversely, too small grain size may result in a higher degree of cation mixing and lower hexagonal ordering [17]. However, the effects of aforesaid phenomenon jointly on material performance have not been systematically studied. In addition, the critical factors influencing the performance of $LiNi_xCo_yMn_zO_2$ cathode materials needs to be researched further.

In this paper, layered $Li_{1.06}Ni_{0.5}Co_{0.2}Mn_{0.3}O_2$ materials are synthesized by synthesizing precursors with a certain amount of Li_2CO_3 at different temperatures. The morphology, structural properties, and electrochemical performance of these samples are compared to determine the optimum synthesis temperature for $Li_{1.06}Ni_{0.5}Co_{0.2}Mn_{0.3}O_2$. We examine the influence of synthesis temperature on particle size, the degree of cation mixing, and crystalline structure, and find out which factors determine the performance of $Li_{1.06}Ni_{0.5}Co_{0.2}Mn_{0.3}O_2$.

2. EXPERIMENTAL

The precursor $Ni_{0.5}Co_{0.2}Mn_{0.3}(OH)_2$ was prepared by co-precipitation. $NiSO_4 \cdot 6H_2O$, $CoSO_4 \cdot 7H_2O$, and $MnSO_4 \cdot H_2O$ (molar ratio of Ni/Co/Mn=5:2:3) were used as the starting materials. After the temperature of distilled water in the stirred tank reactor reached 55 °C, NaOH solution (4 M), $NH_3 \cdot H_2O$ (0.34 M), and transition metal sulfate solution (2 M) were pumped into the reactor under nitrogen protection, then reacted for 10h. The pH was carefully controlled at 11. After filtering, washing the as-prepared hydroxide precursor three times by distilled water, and drying at 120 °C for 12 h, the obtained hydroxide precursor was ground for 20 min with a certain amount of Li_2CO_3 by adding alcohol to a mortar until the liquid volatilized. The mixed powders were heated at 500 °C for 5 h and then synthesized in air at 800, 850, 900, 920, 940, or 980 °C, respectively. The technological component for each metal in $Li_{1.06}Ni_{0.5}Co_{0.2}Mn_{0.3}O_2$ measured by inductively coupled plasma (ICP) spectroscopy is the same as that of stoichiometry.

The crystalline structure of powder samples was analyzed by X-ray diffraction (XRD; D/Max2500PC, Japan) with Cu Kα radiation (λ=1.5406 Å) for 1 s at each 0.02° step width over the two Theta degree scan range from 10° to 120°. Sample morphology was observed by scanning electron microscopy (SEM).

CR2016 coin cells were assembled using Li foil as the anode and $Li_{1.06}Ni_{0.5}Co_{0.2}Mn_{0.3}O_2$ as the cathode in a glove box. Each cathode slurry was prepared by mixing 85 wt. % active material, 9 wt. %

acetylene black, and 6 wt. % polyvinylidene fluoride in N-methyl-2-pyrrolidone solution by magnetic stirring for 5 h. The slurry was coated onto an aluminum foil and then dried at 120 °C for 12 h under vacuum. A 1 M solution of $LiPF_6$ dissolved in ethylene carbonate and dimethyl carbonate (1:1 v/v) was used as the electrolyte. Charge–discharge measurements were conducted by LAND-CT2001A system (Wuhan, China), in the range of 2.5–4.2 V, 2.5–4.3 V, and 2.5–4.5 V at 0.1C, 1C, and 2C, respectively. Electrochemical impedance spectroscopy (EIS) was analyzed on an IM6/Zennium apparatus (Zahner, Germany) in the frequency range from 10^5 to 10^{-2} Hz, and the amplitude of the AC signal was 5 mV. All the experiments were operated at room temperature.

3. RESULTS

Fig. 1 shows SEM images of the $Li_{1.06}Ni_{0.5}Co_{0.2}Mn_{0.3}O_2$ samples synthesized at different temperatures. All of the secondary grains presented a typical spherical morphology with a narrow particle size distribution. The average particle sizes of the six samples were nearly the same as each other, about 10 μm. However, synthesis temperature clearly influenced the primary particle size. The primary particle size for each sample was measured by calculating the average value of more than 30 primary particles and is displayed in Fig. 2. Increasing the synthesis temperature from 800 to 900 °C induced a minor increase in primary particle size from 0.45 to 0.61 μm. Upon raising the temperature to 980 °C, the primary particle size increased rapidly to 1.77 μm. That is, a higher synthesis temperature resulted in a larger primary particle size.

Fig. 3 shows the XRD patterns of $Li_{1.06}Ni_{0.5}Co_{0.2}Mn_{0.3}O_2$ samples synthesized at different temperatures to demonstrate the relationship between synthesis temperature and crystal structure. All the peaks could be well indexed to a hexagonal α-NaFeO₂ structure with R-3m space group [18]. Furthermore, no impurity peaks were observed between 20° and 25°, indicating that pure $Li_{1.06}Ni_{0.5}Co_{0.2}Mn_{0.3}O_2$ samples without by-products were obtained [19,20]. With increasing synthesis temperature, the main peaks become sharper and the (006)/(102) and (108)/(110) peaks split more clearly, confirming the formation of a highly ordered layered structure [21].
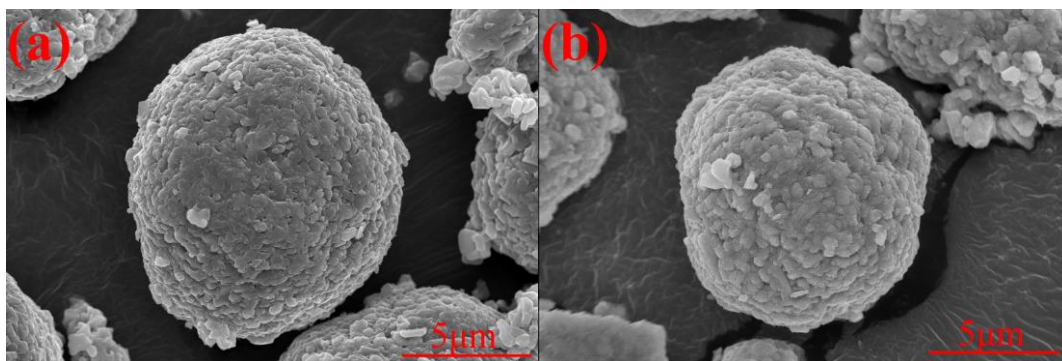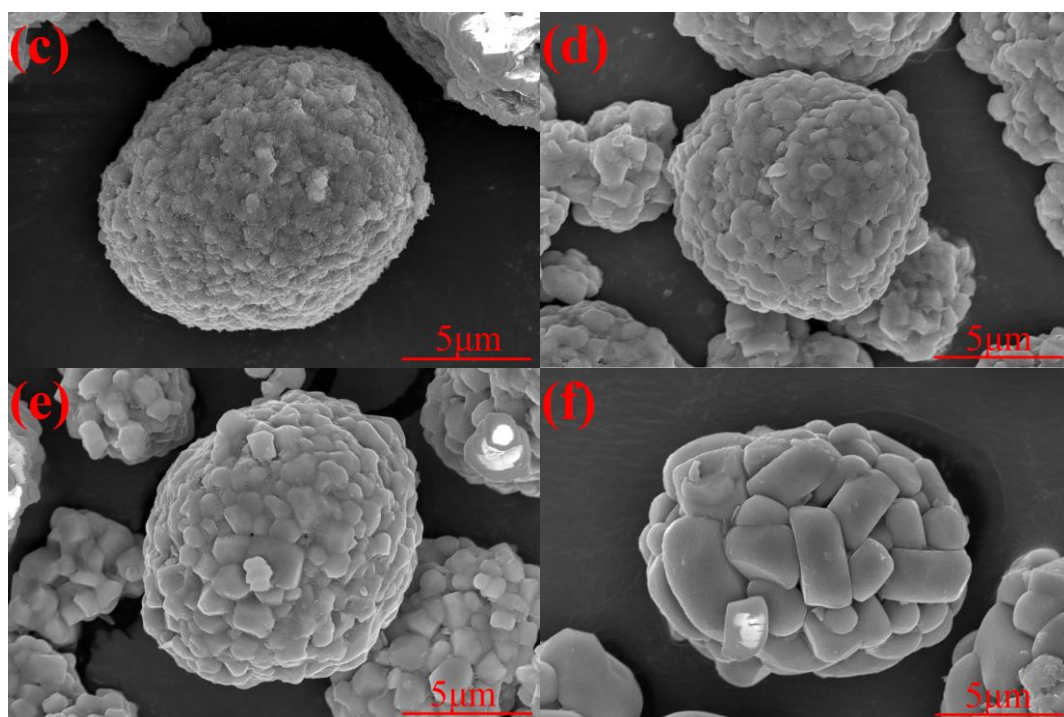
Figure 1. SEM images of $Li_{1.06}Ni_{0.5}Co_{0.2}Mn_{0.3}O_2$ samples synthesized at (a) 800 °C, (b) 850 °C, (c) 900 °C, (d) 920 °C, (e) 940 °C, and (f) 980 °C.

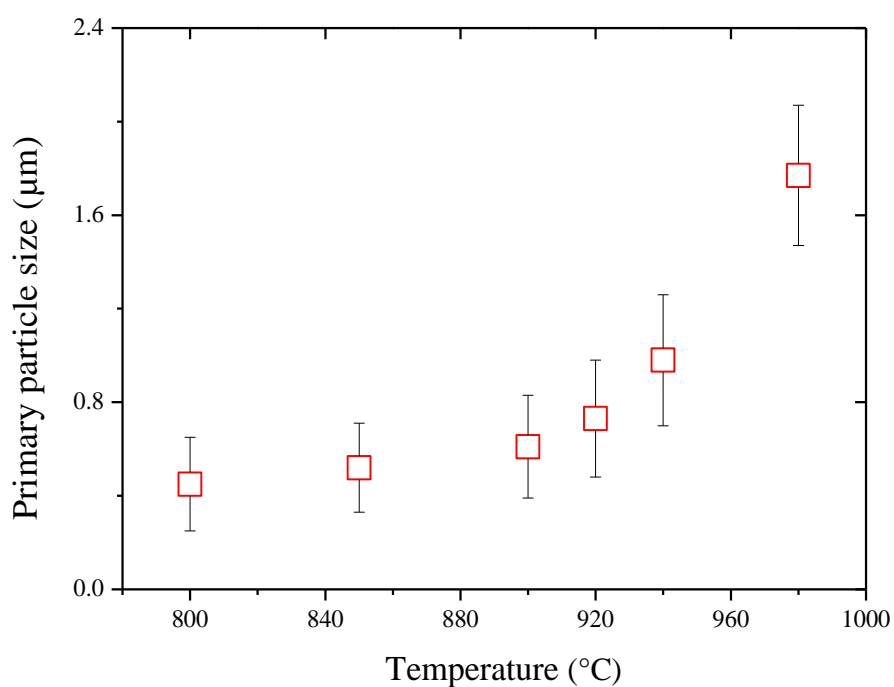**Figure 2.** Primary particle size of $Li_{1.06}Ni_{0.5}Co_{0.2}Mn_{0.3}O_2$ samples synthesized at different temperatures measured by determining the average values for more than 30 primary particles.
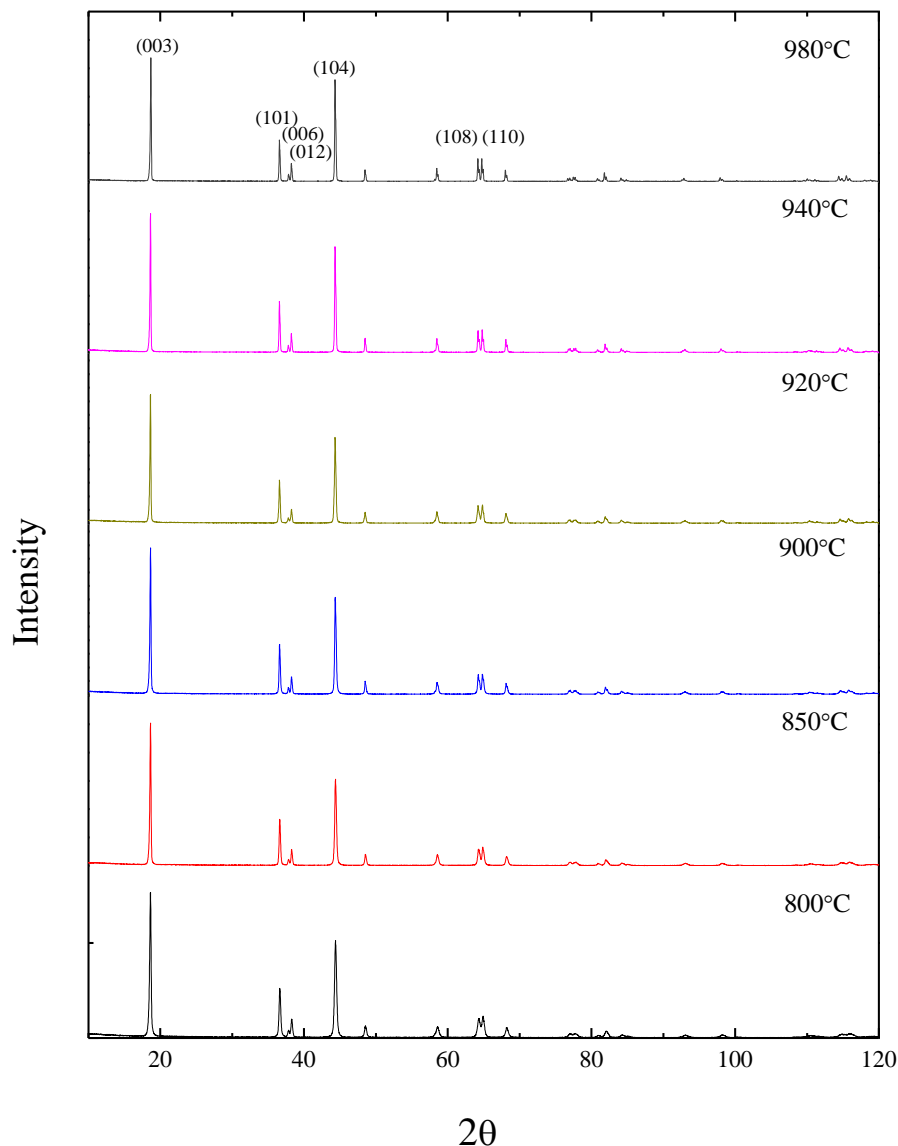
Figure 3. XRD patterns of $Li_{1.06}Ni_{0.5}Co_{0.2}Mn_{0.3}O_2$ samples synthesized at different temperatures.

The XRD patterns of the $Li_{1.06}Ni_{0.5}Co_{0.2}Mn_{0.3}O_2$ samples synthesized at different temperatures were refined. The XRD pattern of $Li_{1.06}Ni_{0.5}Co_{0.2}Mn_{0.3}O_2$ synthesized at 900 °C together with its refinement is shown in Fig. 4.
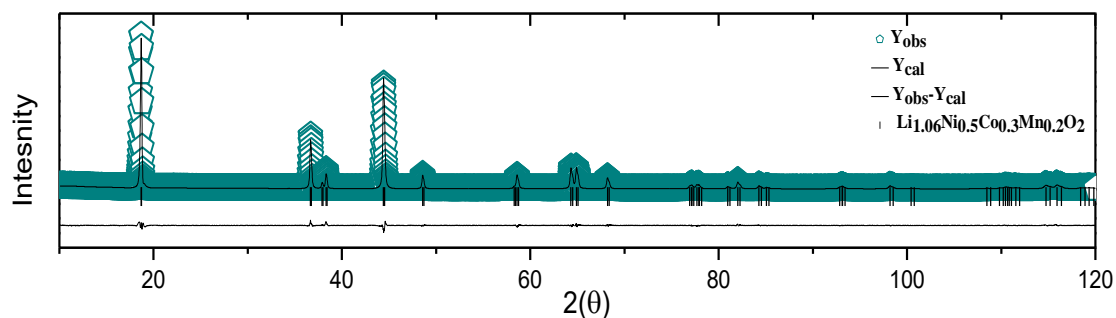
Figure 4. Comparison of the experimental and calculated XRD patterns of $Li_{1.06}Ni_{0.5}Co_{0.2}Mn_{0.3}O_2$
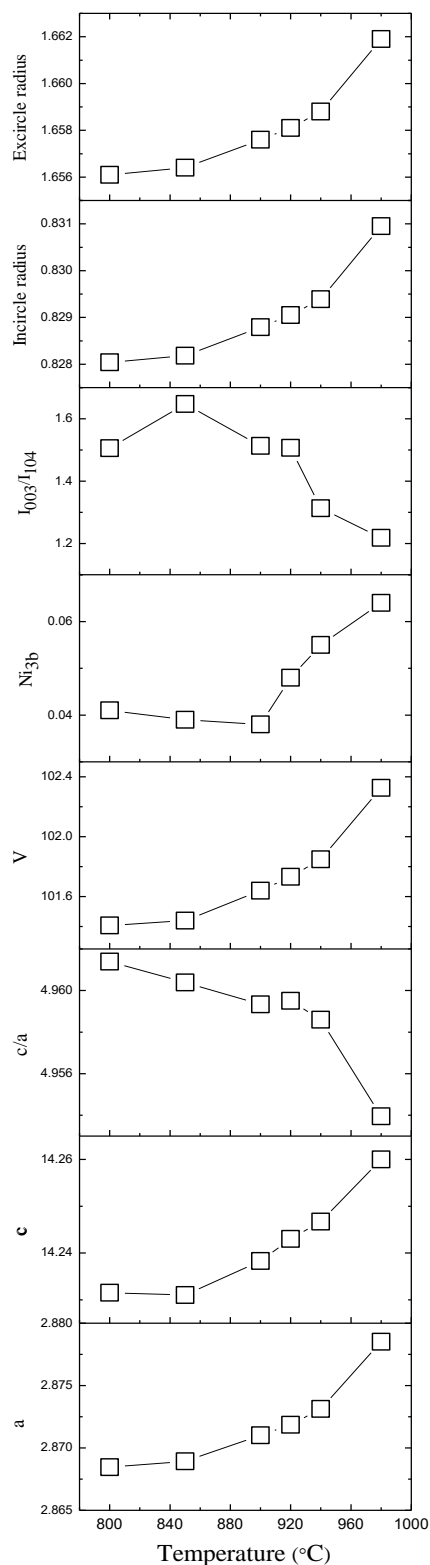
Figure 5. Lattice parameters *a* and *c*, *c/a* ratio, volume, content of Ni_{3b}, ratio of I_{003}/I_{104}, and the size of the incircle/circumcircle radii of the tetrahedral sites of $Li_{1.06}Ni_{0.5}Co_{0.2}Mn_{0.3}O_2$ samples synthesized at different temperatures.

Detailed lattice parameters are presented in Fig. 5 and Table 1 from the refinement of the XRD data. As the synthesis temperature rose, the lattice parameters *a* and *c* (except for the sample

synthesized at 850 °C) and cell volume increased progressively. It is generally accepted that the intensity ratio of I_{003}/I_{104} is sensitive to the degree of cation disorder between Li^+ and Ni^{2+} [22-24]. Ordinarily, the higher the I_{003}/I_{104} ratio, the lower the level of cation mixing. For our $Li_{1.06}Ni_{0.5}Co_{0.2}Mn_{0.3}O_2$ samples, with increasing synthesis temperature from 800 to 980 °C, the value of I_{103}/I_{104} first increased to reach a maximum value of 1.64715 at 850 °C, and then decreased. This means the sample synthesized at 850 °C has the lowest cation mixing of the samples. However, when the synthesis temperature was 900 °C, the content of nickel ions at the 3b site (Ni_{3b}) was the lowest of the samples (0.038), which is inconsistent with the aforementioned results for the I_{003}/I_{104} ratio. The valence of the nickel ion at the 3b site was reported to be 2+ [25]. The lower the value of Ni_{3b}, the lower the disorder of Ni^{2+} and Li^+, which proves that the sample synthesized at 900 °C possesses the lowest cation mixing rather than that synthesized at 850 °C. These results also reveal that the I_{003}/I_{104} ratio can be used to qualitatively analyze cation mixing, albeit with low precision.

Table 1. Structural parameters of $Li_{1.06}Ni_{0.5}Co_{0.2}Mn_{0.3}O_2$ samples synthesized at different temperatures determined from the refinement of XRD data.

		800	850	900	920	940	980
Space group		R-3m	R-3m	R-3m	R-3m	R-3m	R-3m
Lattice constants							
a		2.86845(9)	2.86893(7)	2.87101(6)	2.87186(5)	2.87313(4)	2.87851(3)
b		2.86845(9)	2.86893(7)	2.87101(6)	2.87186(5)	2.87313(4)	2.87851(3)
c		14.2315(5)	14.2310(4)	14.2383(3)	14.2430(3)	14.2467(2)	14.2600(2)
Cell volume		101.407(0.006)	101.439(0.004)	101.639(0.004)	101.732(0.004)	101.849(0.003)	102.326(0.002)
Structure parameters							
R_p		6.27	6.70	7.24	8.15	8.01	9.25
R_{wp}		9.18	9.24	9.87	11.1	11.3	13.2
Li_{3b}	X	0.00000(0)	0.00000(0)	0.00000(0)	0.00000(0)	0.00000(0)	0.00000(0)
	Y	0.00000(0)	0.00000(0)	0.00000(0)	0.00000(0)	0.00000(0)	0.00000(0)
	Z	0.50000(0)	0.50000(0)	0.50000(0)	0.50000(0)	0.50000(0)	0.50000(0)
	SOF	0.959(1)	0.961(1)	0.962(1)	0.952(2)	0.945(2)	0.936(2)
	B	0.247(154)	0.945(154)	0.521(150)	1.473(176)	1.448(164)	0.531(141)
Ni_{3b}	X	0.00000(0)	0.00000(0)	0.00000(0)	0.00000(0)	0.00000(0)	0.00000(0)
	Y	0.00000(0)	0.00000(0)	0.00000(0)	0.00000(0)	0.00000(0)	0.00000(0)
	Z	0.50000(0)	0.50000(0)	0.50000(0)	0.50000(0)	0.50000(0)	0.50000(0)
	SOF	0.041(1)	0.039(1)	0.038(1)	0.048(2)	0.055(2)	0.064(2)
	B	0.247(154)	0.945(154)	0.521(150)	1.473(176)	1.448(164)	0.531(141)
Ni_{3a}	X	0.00000(0)	0.00000(0)	0.00000(0)	0.00000(0)	0.00000(0)	0.00000(0)
	Y	0.00000(0)	0.00000(0)	0.00000(0)	0.00000(0)	0.00000(0)	0.00000(0)
	Z	0.00000(0)	0.00000(0)	0.00000(0)	0.00000(0)	0.00000(0)	0.00000(0)
	SOF	0.444(0)	0.446(0)	0.447(0)	0.437(0)	0.43(0)	0.421(0)
	B	0.439(37)	0.389(29)	0.385(27)	0.194(30)	0.344(27)	0.515(27)

Mn$_{3a}$	X	0.00000(0)	0.00000(0)	0.00000(0)	0.00000(0)	0.00000(0)	0.00000(0)
	Y	0.00000(0)	0.00000(0)	0.00000(0)	0.00000(0)	0.00000(0)	0.00000(0)
	Z	0.00000(0)	0.00000(0)	0.00000(0)	0.00000(0)	0.00000(0)	0.00000(0)
	SOF	0.291(0)	0.291(0)	0.291(0)	0.291(0)	0.291(0)	0.291(0)
	B	0.439(37)	0.389(29)	0.385(27)	0.194(30)	0.344(27)	0.515(27)
Co$_{3a}$	X	0.00000(0)	0.00000(0)	0.00000(0)	0.00000(0)	0.00000(0)	0.00000(0)
	Y	0.00000(0)	0.00000(0)	0.00000(0)	0.00000(0)	0.00000(0)	0.00000(0)
	Z	0.00000(0)	0.00000(0)	0.00000(0)	0.00000(0)	0.00000(0)	0.00000(0)
	SOF	0.194(0)	0.194(0)	0.194(0)	0.194(0)	0.194(0)	0.194(0)
	B	0.439(37)	0.389(29)	0.385(27)	0.194(30)	0.344(27)	0.515(27)
Li$_{3a}$	X	0.00000(0)	0.00000(0)	0.00000(0)	0.00000(0)	0.00000(0)	0.00000(0)
	Y	0.00000(0)	0.00000(0)	0.00000(0)	0.00000(0)	0.00000(0)	0.00000(0)
	Z	0.00000(0)	0.00000(0)	0.00000(0)	0.00000(0)	0.00000(0)	0.00000(0)
	SOF	0.071(0)	0.068(0)	0.067(0)	0.077(0)	0.084(0)	0.091(0)
	B	0.439(37)	0.389(29)	0.385(27)	0.194(30)	0.344(27)	0.515(27)
O	X	0.00000(0)	0.00000(0)	0.00000(0)	0.00000(0)	0.00000(0)	0.00000(0)
	Y	0.00000(0)	0.00000(0)	0.00000(0)	0.00000(0)	0.00000(0)	0.00000(0)
	Z	0.25842(11)	0.25870(10)	0.25860(11)	0.25831(12)	0.25821(13)	0.25927(15)
	SOF	1.000(0)	1.000(0)	1.000(0)	1.000(0)	1.000(0)	1.000(0)
	B	1.539(53)	1.508(46)	1.539(47)	1.247(51)	1.611(51)	1.743(55)

The electrochemical performance of $Li_{1.06}Ni_{0.5}Co_{0.2}Mn_{0.3}O_2$ samples synthesized at different temperatures from 800 to 980 °C is compared in Fig. 6 and Table 2–4. Fig. 6a shows initial charge–discharge capacities of the six samples at 0.1C in the range of 2.5–4.2 V. All the discharge curves contain an obvious potential plateau at 3.75 V, which is consistent with the Ni^{2+}/Ni^{4+} redox couple [26]. Table 2 presents the detailed charge–discharge capacity results at 0.1C, 0.5C, and 1C. At 0.1C, the initial discharge capacities of $Li_{1.06}Ni_{0.5}Co_{0.2}Mn_{0.3}O_2$ were 125, 131, 144, 147.7, 136.6, and 103.5 mAhg^{-1} for samples synthesized at 800, 850, 900, 920, 940, and 980 °C, respectively. Both charge and discharge capacities increased gradually with rising synthesis temperature from 800 to 920 °C. Capacity then swiftly decreased as the temperature was elevated from 920 to 980 °C. The initial coulombic efficiencies of these samples was also obviously influenced by synthesis temperature; efficiencies were 73.4%, 74.2%, 81.3%, 82.3%, 78.4%, and 63.0% for samples synthesized at temperatures of 800, 850, 900, 920, 940, and 980 °C, respectively. Amongst the samples, that synthesized at 920 °C exhibited best electrochemical performance with the highest charge–discharge capacity and initial coulomb efficiency. Moreover, it displayed capacities of 122.2 and 105.8 mAhg^{-1} at 0.5C and 1C, respectively, after ten cycles, showing superior cycle stability and rate capability compared with those of the other samples.

Fig. 6b illustrates the initial charge and discharge capacities of the samples at 0.1C between 2.5 and 4.3 V; the corresponding cycling performance and rate capability are presented in Table 3. Synthesis temperature exerts a larger effect on capacity than on coulomb efficiency. Resembling the behavior at 2.5–4.2 V, samples synthesized at 800, 850, 900, 920, 940, and 980 °C displayed discharge capacities of 154.2, 160.4, 173.5, 178.6, 163.1, and 133.8 mAhg^{-1}, respectively, and initial coulomb efficiencies of 77.8%, 80.2%, 82.7%, 83.8%, 82.5%, and 72.8%.
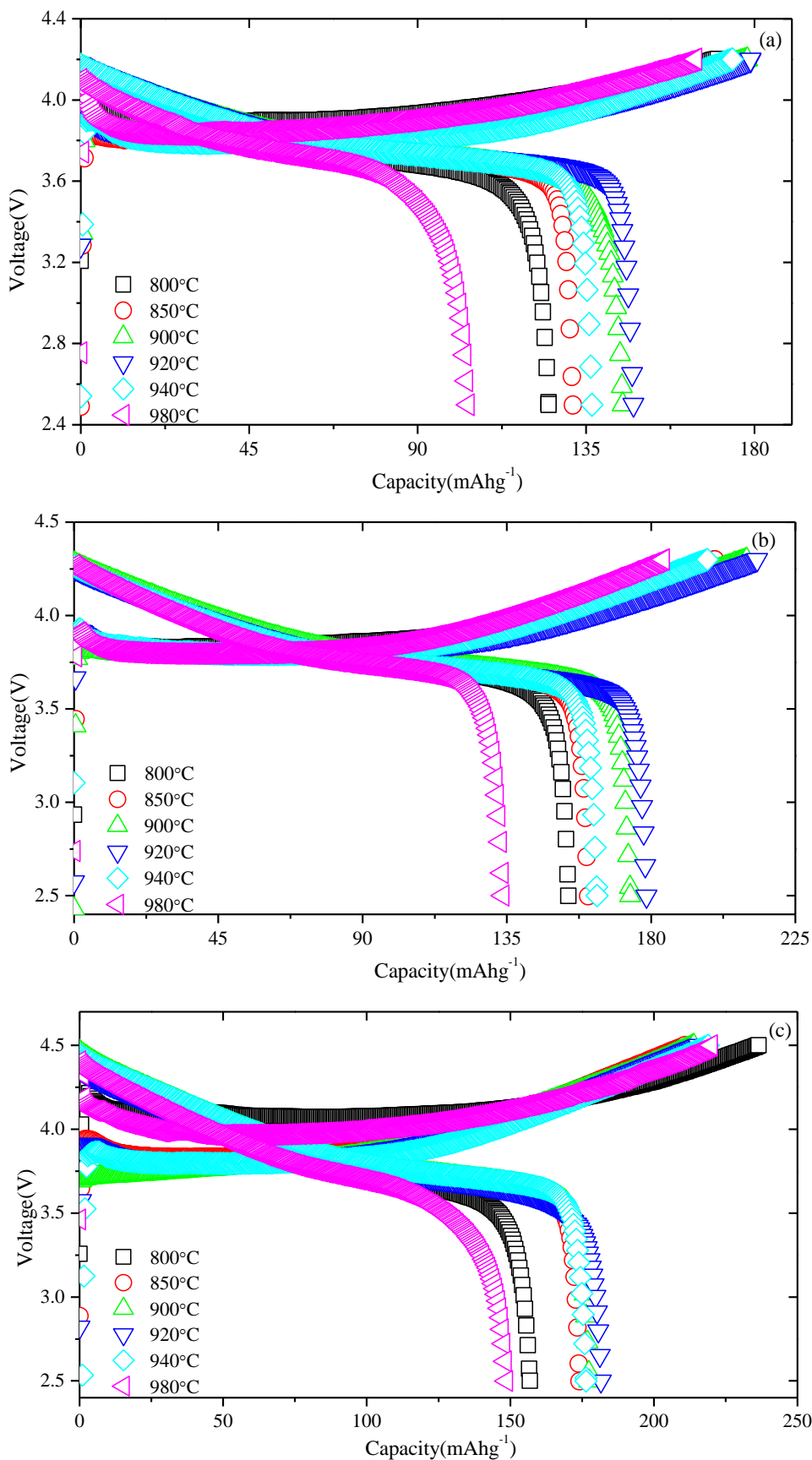
Figure 6. Initial charge–discharge capacities of $Li_{1.06}Ni_{0.5}Co_{0.2}Mn_{0.3}O_2$ samples synthesized at different temperatures at 0.1 C in the ranges of (a) 2.5–4.2 V, (b) 2.5–4.3 V, and (c) 2.5–4.5 V.

Table 2. Charge–discharge capacities and coulombic efficiencies of $Li_{1.06}Ni_{0.5}Co_{0.2}Mn_{0.3}O_2$ samples synthesized at different temperatures at 0.1C, 0.5C, and 1C between 2.5 and 4.2 V.

T (°C)	Initial cycle (0.1C)				0.5C		1C	
	charge $(mAhg^1)$	discharge $(mAhg^{-1})$	Coulombic efficiency (%)	10th discharge $(mAhg^{-1})$	1st discharge $(mAhg^{-1})$	10th discharge $(mAhg^{-1})$	1st discharge $(mAhg^{-1})$	10th discharge $(mAhg^{-1})$
800	170.2	125.0	73.4	131.2	111.9	111.3	91.2	93.4
850	177.2	131.5	74.2	136.9	114.2	112.0	96.2	92.3
900	178.1	144.8	81.3	144.6	119.2	118.6	101.3	100.6
920	179.5	147.7	82.3	155.1	122.8	122.2	107.3	105.8
940	174.1	136.6	78.4	137.8	106.9	106.2	75.4	74.2
980	164.3	103.5	63.0	99.5	72.3	75.1	49.6	47.4

Table 3. Charge–discharge capacities and coulombic efficiencies of $Li_{1.06}Ni_{0.5}Co_{0.2}Mn_{0.3}O_2$ samples synthesized at different temperatures at 0.1C, 0.5C, and 1C between 2.5 and 4.3 V.

T (°C)	Initial cycle (0.1C)				0.5C		1C	
	charge $(mAhg^{-1})$	discharge $(mAhg^{-1})$	Coulombic efficiency (%)	10th discharge $(mAhg^{-1})$	1st discharge $(mAhg^{-1})$	10th discharge $(mAhg^{-1})$	1st discharge $(mAhg^{-1})$	10th discharge $(mAhg^{-1})$
800	198.2	154.2	77.8	150.2	115.9	121.2	97.7	103.9
850	199.9	160.4	80.2	160.8	137.0	139.3	118.7	121.2
900	209.8	173.5	82.7	170.0	142.6	146.8	126.2	131.2
920	213.1	178.6	83.8	176.4	148.8	151.7	130.2	134.3
940	197.6	163.1	82.5	156.4	121.3	123.0	100.8	104.8
980	183.3	133.8	72.8	120.2	85.5	84.5	62.2	59.4

Table 4. Charge–discharge capacities and coulombic efficiencies of $Li_{1.06}Ni_{0.5}Co_{0.2}Mn_{0.3}O_2$ samples synthesized at different temperatures at 0.1C, 0.5C, and 1C between 2.5 and 4.5 V.

T (°C)	Initial cycle (0.1C)				0.5C		1C	
	charge $(mAhg^{-1})$	discharge $(mAhg^{-1})$	Coulombic efficiency (%)	10th discharge $(mAhg^{-1})$	1st discharge $(mAhg^{-1})$	10th discharge $(mAhg^{-1})$	1st discharge $(mAhg^{-1})$	10th discharge $(mAhg^{-1})$
800	236.5	156.8	66.3	163.6	135.3	128.8	113.1	108.6
850	210.9	174.1	82.5	180.5	152.2	145.0	127.4	124.7
900	213.9	177.5	83.0	183.9	157.3	150.0	137.4	134.1
920	215.6	181.6	84.2	194.9	167.8	157.5	141.3	137.3
940	218.9	176.4	80.6	177.1	144.3	134.2	116.9	112.0
980	220.0	148.7	67.6	126.8	83.2	82.9	55.3	47.8

Again, these parameters increased below 920 °C and then decreased. Similarly, in the large voltage range between 2.5 and 4.5 V, the $Li_{1.06}Ni_{0.5}Co_{0.2}Mn_{0.3}O_2$ sample synthesized at 920 °C exhibited the highest discharge capacity of 181.6 mAhg^{-1} and highest initial coulomb efficiency of 84.2% compared with those of the other samples, as summarized in Fig. 6c and Table 4.

EIS data for the $Li_{1.06}Ni_{0.5}Co_{0.2}Mn_{0.3}O_2$ materials were measured to determine the effect synthesis temperature on impedance. Fig. 7 presents the EIS data for cells containing samples synthesized at different temperatures after ten cycles between 2.5 and 4.5 V. Each spectrum consists of two semicircles at high to medium frequency and a straight line at low frequency. The intersection of the first semicircle with the lateral axis represents the electrolyte resistance (R_e). The first semicircle at high frequency is associated with resistance of the solid–electrolyte interface (R_{sf}).
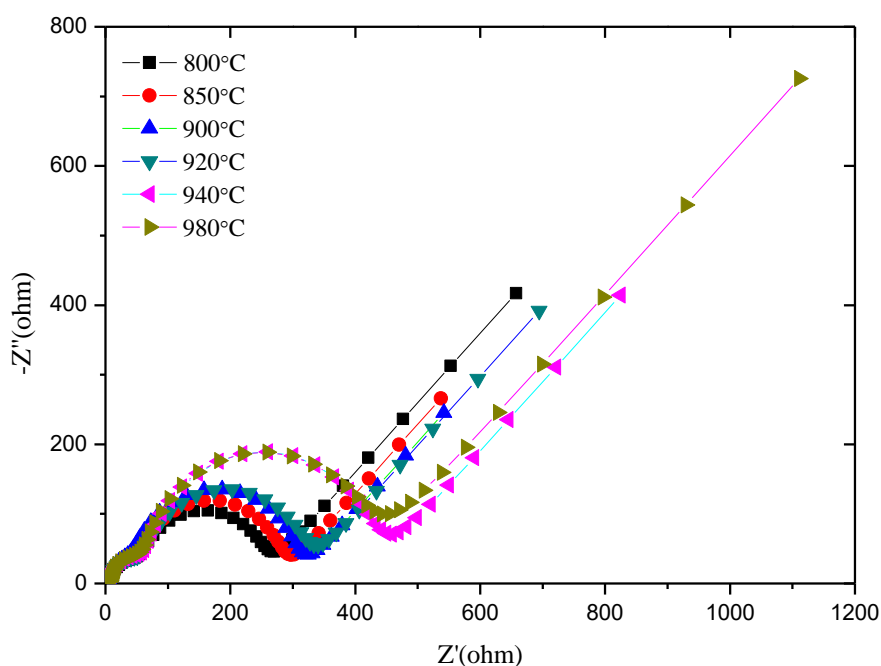

Figure 7. Nyquist plots of $Li_{1.06}Ni_{0.5}Co_{0.2}Mn_{0.3}O_2$ samples synthesized at different temperatures after ten cycles between 2.5 and 4.5 V at 0.1C.
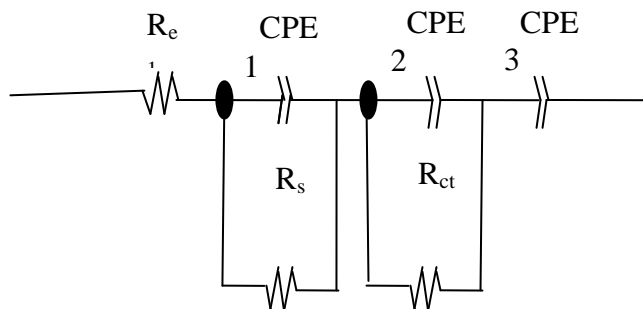

Figure 8. Equivalent circuit used to fit the experimental data.

Table 5. Equivalent circuit parameters obtained using the simulated AC impedance after ten cycles between 2.5 and 4.5 V.

T(°C)	$R_e(\Omega)$	$R_{sf}(\Omega)$	$R_{ct}(\Omega)$
800	7.333	43.87	189.2
850	6.48	42.86	222.1
900	4.085	38.22	254.4
920	6.902	48.59	275.8
940	6.255	49.62	326.5
980	5.931	46.96	332.6

The second semicircle at intermediate frequency corresponds to the charge-transfer resistance (R_{ct}). Fig. 8 depicts the equivalent circuit used to fit the EIS data and the values of R_e, R_{sf}, and R_{ct} are presented in Table 5. By and large, R_{ct} increases with synthesis temperature from 800 to 980 °C, while R_{sf} values are roughly equal.

4. DISCUSSION

The content of Ni_{3b} first decreased from 0.041 to 0.038 and then increased to 0.064 as the synthesis temperature rose from 800 to 980° C, reaching its lowest value of 0.038 for the sample synthesized at 900 °C. Because the ionic radii of Li^+ and Ni^{2+} are nearly the same, Li^+ and Ni^{2+} often mix substantially in the crystal lattice [13-14]. This phenomenon blocks the pathways for lithium-ion diffusion, which lowers electrochemical performance. Therefore, the electrochemical properties of samples may improve and then degrade with increasing synthesis temperature from 800 to 980 °C because of the level of cation mixing in the crystal lattice. In the layered $LiNi_xCo_yMn_zO_2$ crystalline structure, the oxygen atoms are arranged in a slightly distorted, cubic close-packed arrangement, while the transition metal and lithium ions occupy the center positions of oxygen octahedra [27]. Fig. 9 shows a schematic diagram of lithium-ion migration in the layered $LiNi_xCo_yMn_zO_2$ crystalline structure. Lithium ions migrate from an octahedral site in the lithium layer into an adjacent octahedral site through an empty tetrahedral site [28]. Thus, the size of the tetrahedral site plays an important role in the delithiation/lithiation process. A larger space gives rise to faster lithium-ion diffusion. The incircle/circumcircle radii of the tetrahedral site were evaluated from the Rietveld refinement shown in Fig. 5. As the synthesis temperature rose from 800 to 980 °C, the incircle radius increased gradually from 0.82804 to 0.83905 Å, while the circumcircle radius increased from 1.6561 to 1.6619 Å. Therefore, raising the synthesis temperature could broaden the size of the tetrahedral site, facilitating lithium-ion migration and improving electrochemical performance. Raising the synthesis temperature from 800 to 980 °C caused the primary particle size to increase from 0.45 to 1.77 μm. A smaller primary particle size results in larger specific surface area, which facilitates the extraction and insertion of lithium-ion at the powder interface; the lithium-ion diffusion kinetics become slow for large

particles [16]. As a result, the materials synthesized at lower temperature with smaller primary particle size may possess better electrochemical properties.
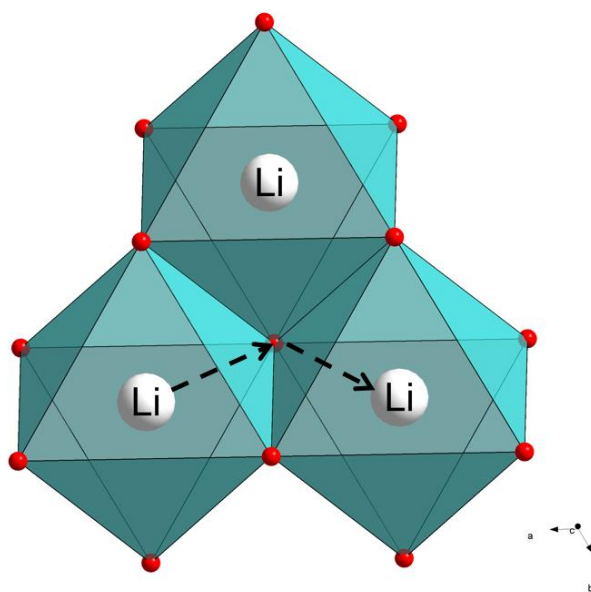

Figure 9. Schematic diagram of lithium-ion migration in the layered $LiNi_xCo_yMn_zO_2$ structure.

The electrochemical performance of $Li_{1.06}Ni_{0.5}Co_{0.2}Mn_{0.3}O_2$ samples improved for those synthesized at 800 to 920 °C, and then began to degrade as the temperature rose to 980 °C. This variation of electrochemical performance is roughly consistent with the change of Ni_{3b} with increasing synthesis temperature. Therefore, the level of cation mixing strongly influences electrochemical performance. The sample with the lowest level of cation mixing (that synthesized at 900 °C) is expected to exhibit best electrochemical properties of the samples. However, it is the sample synthesized at 920 °C that shows the optimal electrochemical performance even though it possesses a higher Ni_{3b} content than those of samples synthesized at 800, 850, and 900 °C. Therefore, another important factor contributes to the electrochemical performance of the samples that causes the optimum synthesis temperature to shift from 900 to 920 °C. Considering the variations of primary particle size and the size of tetrahedral sites with synthesis temperature and their effects on the electrochemical properties of the samples, the former could cause the optimum synthesis temperature to shift to lower temperature, whereas the latter should make it shift to higher temperature. Therefore, the electrochemical performance of $LiNi_xCo_yMn_zO_2$ materials chiefly depends on the level of cation mixing and the incircle/circumcircle radii of tetrahedral sites rather than primary particle size.

5. CONCLUSIONS

Layered $Li_{1.06}Ni_{0.5}Co_{0.2}Mn_{0.3}O_2$ cathode materials were prepared by co-precipitation, and the relationship between synthesis temperature and the crystal structure and electrochemical properties of materials was studied. The primary particle size of the powders increased gradually with rising

synthesis temperature. The concentration of Ni^{2+}-3b ions reached its minimum value of 0.038 for the sample synthesized at 900 °C. The $Li_{1.06}Ni_{0.5}Co_{0.2}Mn_{0.3}O_2$ sample synthesized at 920 °C exhibited the best electrochemical performance of the samples, delivering the highest discharge capacity of 181.6m Ahg^{-1} and initial coulombic efficiency of 84.2% at 0.1C between 2.5 and 4.5 V. The size of tetrahedral sites providing space for lithium-ion diffusion was evaluated; higher sintering temperature resulted in bigger incircle/circumcircle radii of the tetrahedral sites. These results indicate that the electrochemical performance of $Li_{1.06}Ni_{0.5}Co_{0.2}Mn_{0.3}O_2$ mainly depends on the level of cation mixing and the size of tetrahedral sites rather than primary particle size.

References

1. M.C. Lin, M. Gong, B.G. Lu, Y.P. Wu, D.Y. Wang, M.Y. Guan, M. Angell, C.X. Chen, J. Yang, B.J. Hwang and H.J. Dai, *Nature*, 520 (2015) 324.
2. M. Armand and J.-M. Tarascon, *Nature*, 451 (2008) 652.
3. M.S. Whittingham, *Chem. Rev.*, 104 (2004) 4271.
4. Y.-K. Sun, C.S. Yoon, S.-T. Myung, I. Belharouak and K. Amine, *J. Electrochem. Soc.*, 156 (2009) A1005.
5. J.M. Tarascon, D. Guyomard and G.L. Baker, *J. Power Sources*, 44 (1993) 689.
6. J. Breger, N. Dupre ´, P.J. Chupas, P.L. Lee, T. Proffen, J.B. Parise and C.P. Grey, *J. Am. Chem. Soc.*, 127 (2005) 7529.
7. L.J. Li, X.H. Li, Z.X. Wang, H.J. Guo, P. Yue, W. Chen and L. Wu, *J. Alloys Compd.*, 507 (2010) 172.
8. J.J. Liu, W.H. Qiu, L.Y. Yu, H.L. Zhao and T. Li, *J. Alloys Compd.*, 449 (2008) 326.
9. H.B. Ren, X. Li and Z.H. Peng, *Electrochim. Acta*, 56 (2011) 7088.
10. K.C. Wu, F. Wang, L.L. Gao, M.R. Li, L.L. Xiao, L.T. Zhao, S.J. Hu, X.J. Wang, Z.L. Xu and Q.G. Wu, *Electrochim. Acta*, 75 (2012) 393.
11. Z.L. Xu, L.L. Xiao, F. Wang, K.C. Wu, L.T. Zhao, M.R. Li, H.L. Zhang, Q.G. Wu and J.B. Wang, *J. Power Sources*, 248 (2014) 180.
12. K. Kang, Y.S. Meng, J. Bre'ger, C.P. Grey and G. Ceder, *Science*, 311 (2008) 977.
13. K.S. Lee, S.T. Myung, J. Prakash, H. Yashiro and Y.K. Sun, *Electrochim. Acta*, 53 (2008) 3065.
14. P.S. Whitfield, I.J. Davidson, L.M.D. Cranswick, I.P. Swainson and P.W. Stephens, *Solid State Ionics*, 176 (2005) 463.
15. Y. Wang and G. Cao, *Adv. Mater.*, 20 (2008) 2251.
16. T. Drezen, N.-H. Kwon, P. Bowen, I. Teerlinck, M. Isono and I. Exnar, *J. Power Sources*, 174 (2007) 949.
17. S.K. Marthaa, H. Sclar, Z.S. Framowitza, D. Kovachevab, N. Saliyski, Y. Gofera, P. Sharona, E. Golikc, B. Markovskya and D. Aurbach, *J. Power Sources*, 189 (2009) 248.
18. J.N. Reimers, E. Rossen, C.D. Jones and J.R. Dahn, *Solid State Ionics*, 61 (4) (1993) 335.
19. J. Jiang, K.W. Eberman, L.J. Krause and J.R. Dahn, *J. Electrochem. Soc.*, 155 (2005) A635.

20. C.S. Johnson, J.S. Kim, C. Lefief, N. Li, J.T. Vaughey and M.M. Thackeray, *Electrochem. Commun.*, 6 (2004) 1085.
21. S.T. Myung, K. Amine and Y.K. Sun, *J. Mater. Chem.*, 20 (2010) 7074.
22. D.P. Wang, I. Belharouak, G.M. Koenig, G.W. Zhou and K. Amine, *J. Mater. Chem.*, 21 (2011) 9290.
23. J. Liu, W. Qiu, L. Yu, H. Zhao and T. Li, *J. Alloys Compd.*, 449 (2008) 326.
24. J.R. Dahn, U. von Sacken and C.A. Michal, *Solid State Ionics*, 44 (1–2) (1990) 87.
25. Y.J. Gu, Q.G. Zhang, Y.B. Chen, H.Q. Liu, J.X. Ding, Y.M. Wang, H.F. Wang, L. Chen, M. Wang, S.W. Fan, Q.F. Zang and X.L. Yang, *J. Alloys Compd.*, 630 (2015) 316.
26. R. Santhanam and B. Rambabu, *J. Power Sources*, 195 (2010) 4313.
27. T. Nakamura, K. Sakumoto, M. Okamoto, S. Seki, Y. Kobayashi, T. Takeuchi, M. Tabuchi and Y. Yamada, *J. Power Sources*, 174 (2007) 435.
28. B. Qiu, M.H. Zhang, L.J. Wu, J. Wang, Y.G. Xia, D.N. Qian, H.D. Liu, S. Hy, Y. Chen, K. An, Y.M. Zhu, Z.P. Liu and Y.S. Meng, *Nat. Commun.*, 7 (2016) 12108.